RSC Advances

ROYAL SOCIETY OF CHEMISTRY

www.rsc.org/advances

RSC Advances

RSCPublishing

COMMUNICATION

A novel regrowth method to simply prepare Li-doped ZnO nanorods and improve their photoluminescence properties†

Cite this: DOI: 10.1039/x0xx00000x

Received 00th January 2012,
Accepted 00th January 2012

DOI: 10.1039/x0xx00000x

www.rsc.org/MaterialsC

Giwoong Nam, Byunggu Kim, Youngbin Park, Cheoleon Lee, Seonhee Park, Jiyun Moon, and Jae-Young Leem*

In this study, we report the fabrication of sol-gel prepared ZnO nanorods through the use of vapor-confined face-to-face annealing (VC-FTFA) in which mica was inserted between two films, followed by annealing using the FTFA method. LZO nanorods are regrown when lithium chloride is used as the solvent because $ZnCl_2$ and LiCl vapors are generated. The near-band-edge emission intensity of the LZO nanorods is enhanced through annealing using the VC-FTFA method and is increased by a factor of 6 compared to that of LZO thin films annealed in open air at 600 °C. Our method may provide a route toward the facile fabrication of ZnO nanorods.

One-dimensional ZnO nanostructures, including nanorods, nanowires, and nanotubes, have aroused considerable research interest because of their potential applications in optoelectric nanodevices.[1] ZnO, a direct-band-gap (3.37 eV) semiconductor with an exciton binding energy of 60 meV, is a suitable material for optical applications. ZnO nanorods are expected to exhibit enhanced luminescence efficiency because of their high aspect ratios and quantum-confinement effects. For fabrication ZnO-based optoelectronic devices, both n- and p-type materials are required. Group-I elements (Li and Na) and group-V elements (N, P, As, and Sb) were tried as the suitable dopants to realize the p-type conductivity in ZnO. However, acceptor levels of group-V elements are theoretically identified to be deep with low solubility limits. It is predicted theoretically that p-type doping is possible when group-I elements substitute Zn in ZnO lattice, which behave as shallow acceptors.[2] Among group-I elements, lithium is the best candidate in producing p-type ZnO because of almost no lattice relaxations and ZnO LED based on the Li-N codoped p-type ZnO has been fabricated, which can work continuously for 6.8 hours.[3] A number of different techniques have been utilized to prepare ZnO films. The sol-gel method is one of the most attractive processes because of the control it permits over composition, its simple resource requirements, and its low cost. In the sol-gel process, ZnO films are obtained via post-deposition crystallization. The as-deposited films are in an amorphous state and must be transformed into the crystalline state via post-annealing. When sol-gel prepared ZnO films are annealed, the resulting films generally contain crystalline grains with random orientations because of nucleation and crystal growth in the bulk of the films.[4] However, the *c*-axis orientation is of prime importance in Li-doped ZnO (LZO) films, especially for films applied in piezoelectric and ferroelectric devices. Although some research has been conducted regarding Li/ZnO composites, most of this research has focused on the structural and electrical properties of these composites, and only a few reports have focused on the photoluminescence (PL) properties, which are degraded that optical properties of LZO deposited using sol-gel process.[5]

A face-to-face annealing (FTFA) approach is commonly employed for GaAs semiconductors to prevent the out-diffusion of arsenic.[6] The GaAs wafer to be annealed is placed between a bottom Si wafer and a top GaAs wafer with the polished surfaces facing each other, hence the name FTFA. Wang et al.[7] have found that the PL properties of ZnO films can be enhanced by the use of the FTFA method. In this study, we used sol-gel spin-coating and a novel annealing method, vapor-confined FTFA (VC-FTFA), to fabricate LZO nanorods, using lithium chloride to regrow the nanorods. This method has several advantages over the conventional FTFA method, including a sharp increase in the near-band-edge (NBE) emission intensity in the PL spectra. Here, we describe the mechanism for the generation of vapors during annealing and the influence of the confined vapors during the VC-FTFA method on the optical properties of LZO nanorods.

The basic strategy for annealing spin-coated LZO films (12 at.%) is illustrated in Scheme 1. Three samples were prepared at 600 ºC for a comparative study. Sample 1 was annealed in open air. Sample 2 was annealed using the conventional FTFA method, in which two films were placed together in an FTF arrangement during annealing. For sample 3, mica was inserted between the two films, and which were then annealed using the FTFA method.

The thermal-decomposition behaviors of the ZnO and LZO (Li/Zn = 30 at.%) precursors were determined using a thermogravimetry-differential thermal analyzer (TG-DTA); the materials were heated in the TG-DTA from room temperature to 700 ºC at a constant rate of 10 ºC/min in air. Fig. 1 shows the TG-DTA curves of the ZnO and LZO precursors. The TGA curves reveal that the ZnO and LZO precursors exhibited an initial weight loss at 100 ºC, which resulted from the evaporation of the solvent and water. The ZnO and LZO precursors also exhibited weight losses in the temperature regions of

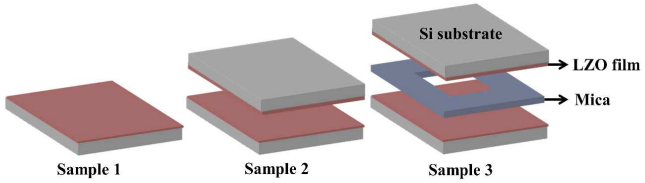

Scheme 1 Schematic illustration of the annealing method. Annealing configurations: FTF without any additional film (sample 1) and with additional film (sample 2). In the schematic diagram of sample 2, mica was inserted between the two films (sample 3).

100 ~ 220 and 220 ~ 250 ºC and of 100 ~ 300, 300 ~ 470, and 470 ~ 600 ºC, respectively, which were attributed to the decomposition of organic compounds. Specifically, in the temperature region of 300 ~ 600 ºC, the LZO precursor slowly evaporated, which generated $ZnCl_2$ and LiCl vapors, as described by the following reactions:

$$Zn(CH_3COO)_2 + 2H_2O \rightarrow Zn(OH)_2 + 2CH_3COOH(\uparrow) \quad (1)$$

$$LiCl + H_2O \rightarrow LiOH + HCl(\uparrow) \quad (2)$$

$$Zn(OH)_2 + LiOH + 3HCl \rightarrow ZnCl_2(\uparrow) + LiCl(\uparrow) + 3H_2O(\uparrow) \quad (3)$$

The ZnO and LZO precursors exhibited endothermic and exothermic peaks between 25 and 300 ºC and between 25 and 550 ºC, respectively, in the heat flow analysis; these peaks were attributed to the evaporation of water and organics from these precursors. The last exothermic peaks in the TG-DTA curves of the ZnO and LZO precursors, at 360 and 600 ºC, respectively, resulted from the crystallization of ZnO and LZO.

Sample 1 consisted of numerous round-shaped ZnO nanoparticles of approximately 60 nm in diameter, as shown in the field-emission scanning electron microscope (FE-SEM) image presented in Fig. 2a. ZnO rods were grown using the FTFA and VC-FTFA methods, and these rods were formed by the round-shaped LZO nanoparticles because of their role in the seed layer. $ZnCl_2$ and LiCl vapors were generated in the temperature region of 300 ~ 600 ºC, and round-shaped nanoparticles were regrown by the $ZnCl_2$ and LiCl vapors. The length of the rods in sample 3 was greater than that in sample 2. The regrowth of the LZO rods can be attributed to the vapor-solid mechanism, in which rods grow via the oxidation of the produced Zn and Li vapors, followed by condensation. The $ZnCl_2$ and LiCl vapors decomposed at 470 ~ 600 ºC, and LZO rods were formed on the round-shaped nanoparticles by organic compounds that contained oxygen or by oxygen present in the air. However, the surface morphology did not change when LZO films were prepared using a lithium acetate (Fig. S1, ESI†), Supporting Information). Therefore, the LZO films were regrown when a chloride-based solvent was

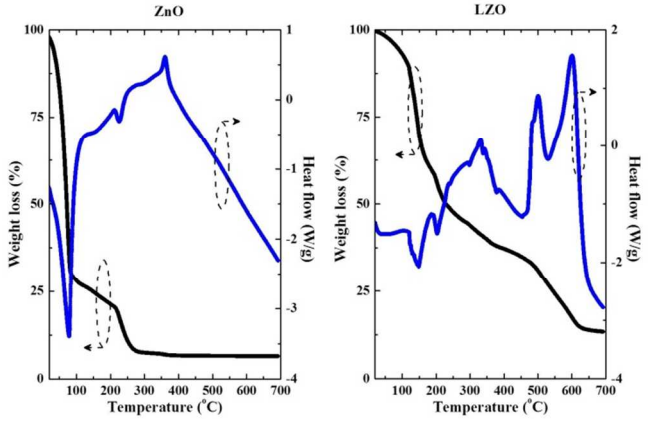

Fig. 1 TGA and DTA curves, shown as the percentage of weight loss and the heat flow, respectively, for the ZnO (left) and LZO (right) precursors.

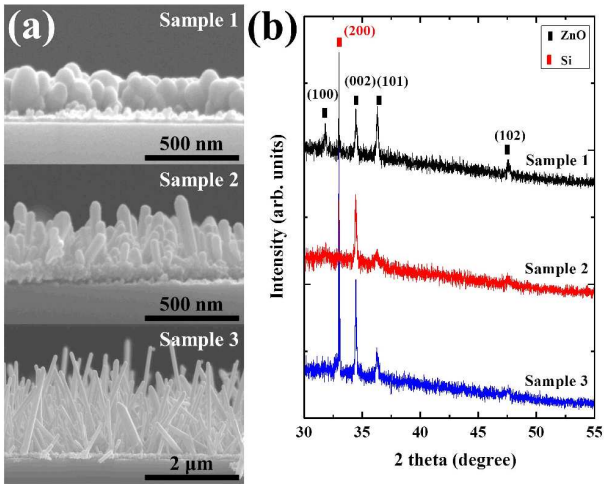

Fig. 2 (a) SEM images and (b) XRD analysis of the three samples.

used because $ZnCl_2$ and LiCl vapors were generated. Fig. 2b shows the X-ray diffraction patterns of the three samples. Four ZnO diffraction peaks were observed at 31º, 34º, 36º, and 47º, which correspond to the (100), (002), (101), and (102) planes, respectively. No traces of Li metal or oxides were detected, indicating that the wurtzite structure was not modified by the incorporation of Li into the ZnO matrix. Samples 2 and 3 exhibited a strong (002) peak, indicating that the c-axis orientation of the ZnO grains was perpendicular to the substrate. It was also observed that the intensity of the (002) peak in sample 3 was larger than that in sample 2.

Fig. 3a presents optical images of the three samples prepared for the comparative study illustrated in Fig. 1. Sample 1 exhibited a

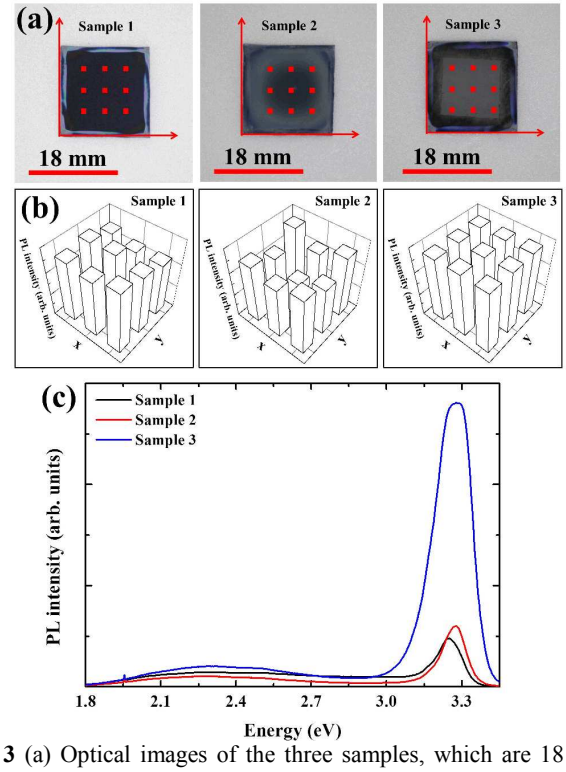

Fig. 3 (a) Optical images of the three samples, which are 18 × 18 mm2 in size. (b) Degree of uniformity of the NBE emission intensities: the PL spectra were measured at the red points in Figure 4a. (c) PL spectra of the LZO films as measured in the centers of samples 1 (black), 2 (red), and 3 (blue).

transparent color, whereas samples 2 and 3 were covered with white-colored products on the surfaces of the Si substrates. We obtained the degree of uniformity of the NBE emission intensities in the PL spectra of the three samples (Fig. 3b) using a continuous-wave helium-cadmium (He–Cd) laser as the optical excitation source, and these intensities were measured at the points marked in red in Fig. 3a. The NBE emission intensities were randomly distributed over the entire surface of sample 1, whereas those of sample 2 were stronger on the edges of the surface than toward the center of the surface because the generated $ZnCl_2$ and LiCl vapors were not sufficiently confined. These vapors remained briefly at the center of the surface, and round-shaped nanoparticles were slightly regrown. For sample 3, however, the NBE emission intensities appeared to be evenly distributed over the entire surface because the vapors were confined by the mica. We attribute the active regrowth to the confinement of these vapors. Fig. 3c presents the PL spectra of the three samples. Notably, the NBE emission intensities of sample 3 are greater than those of samples 1 and 2. The spectra of the three samples contain a green emission band at approximately 2.3 eV that originates from the recombination of holes with the electrons that occupy the singly ionized oxygen vacancies.[8] The regrowth resulting from the VC-FTFA method is effective in increasing not only the NBE emission intensity but also the emission uniformity. The NBE emission intensity of the LZO films annealed in open air, which were deposited using a lithium acetate precursor as the dopant, was similar to that of the LZO films annealed using VC-FTFA method (Fig. S2, ESI†). However, the DL emission of the LZO films annealed using the VC-FTFA method was slightly less than that of the LZO films annealed in open air. This result is similar to that reported by Wang et al.[7], and it is not attributable to regrowth. Therefore, an acetate-based solvent cannot generate vapors that facilitate regrowth. Chloride-containing metals, such as magnesium chloride ($MgCl_2$), can generate $ZnCl_2$ and metal chloride vapors, which were found to lead to an increase in the NBE emission intensity and a blue-shift of the NBE emission peaks (Fig. S3, ESI†). These results are consistent with reaction (3), as presented in Fig. 1.

Fig. S4a (ESI†) presents the PL spectra of LZO films that were annealed using the VC-FTFA method with various annealing temperatures. As the annealing temperature was increased to 600 ºC, the NBE emission intensity also increased. The NBE emission intensity of the film annealed at 500 ºC was the lowest because insufficient amounts of $ZnCl_2$ and LiCl vapors were generated and decomposed only minimally. At an annealing temperature of 600 ºC, $ZnCl_2$ and LiCl vapors were fully generated and decomposed, and these vapors remained between the LZO films and caused active regrewth. The NBE emission intensity, however, decreased as the annealing temperature was increased to 800 ºC because the $ZnCl_2$ and LiCl vapors activated by the thermal energy were not well confined and escaped from the region between the LZO films. The NBE emission intensity of the LZO films annealed in open air followed a similar trend to that of the LZO films annealed using the VC-FTFA method (Fig. S4b, ESI†). As indicated by the PL spectra of the LZO films annealed in open air and using the VC-FTFA method, the NBE emission intensity was enhanced by annealing using the VC-FTFA method, and it was increased by a factor of 6 compared to the films annealed in open air at 600 ºC. The absorbance of the samples 2 and 3 was greater than that of sample 1 (Fig. S5, ESI†). However, absorbance of the sample 2 was similar to that of the sample 3. Therefore, enhanced NBE emission intensity was caused by effect of Li doping and regrowth through the use of VC-FTFA, not effect of thickness, which decreased the nonradiative recombination defect by Li incorporation and increased the crystallinity.

To investigate the acceptor-related emissions, a low-temperature PL measurement was performed at 12 K, as presented in Fig. S6 (ESI†). Six distinct PL peaks appeared in the spectrum of the ZnO film (Fig. S6a, ESI†) at 3.373, 3.361, 3.321, 3.249, 3.177, and 3.105 eV. The NBE emission peaks at 3.373, 3.361, and 3.321 eV were attributed to the emission of free excitons (FX), neutral-donor-bound excitons (D^0X), and two-electron satellites (TES), respectively.[9] The other peaks at 3.249, 3.177, and 3.105 eV were attributed to the first-, -second, and third-order longitudinal optical phonon replicas of TES (TES-1LO, TES-2LO, and TES-3LO), respectively. It is well known that the LO phonon replicas of TES in ZnO have generally been identified based on the energy interval between a TES and the LO phonon energy ($h\omega_{LO}$ = 72 meV).[10] However, five distinct PL peaks were observed in the spectrum of sample 3 (Fig. S6b, ESI†) at 3.373, 3.354, 3.317, 3.287, and 3.215 eV, which were attributed to the emissions of FX, acceptor-bound excitons (A^0X), free-to-neutral-acceptors (e,A^0), donor-acceptor pairs (DAP), and DAP-1LO, respectively.[11] The peaks associated with A^0X, (e,A^0), and DAP, which are closely related to lithium-related acceptor transitions, were not observed in the PL spectrum of the ZnO film.

In summary, LZO nanorods prepared using the VC-FTFA method exhibit enhanced structural and optical properties with respect to LZO films annealed in open air. The regrowth of the LZO films is caused by chloride-containing dopant, such as lithium chloride, which generates $ZnCl_2$ and LiCl vapors.

Acknowledgement

This research was supported by Basic Science Research Program through the National Research Foundation of Korea (NRF) funded by the Ministry of Education, Science and Technology (No. 2012R1A1B3001837). This research was also supported by Global PH.D Fellowship Program through the National Research Foundation of Korea (NRF) funded by the Ministry of Education (No. 2014H1A2A1018051).

Notes and references

Department of Nano Science & Engineering, Inje University, 197, Inje-ro, Gimhae-si, Gyeongsangnam-do, Republic of Korea
E-mail: jyleem@inje.ac.kr

† Electronic Supplementary Information (ESI) available: Experimental details, additional SEM images, and PL spectra of LZO. See DOI: 10.1039/c000000x/

1 (a) M. H. Huang, S. Mao, H. Feick, H. Yan, Y. Wu, H. Kind, E. Weber, R. Russo, P. Yang, *Science* 2001, **292**, 1897; (b) W. I. Park, G. -C. Yi, M. Kim, S. J. Pennycook, *Adv. Mater.* 2003, **15**, 526.
2 C. H. Park, S. B. Zhang, S. H. Wei, *Phys. Rev. B* 2004, **66**, 073202.
3 J. S. Liu, C. X. Shan, H. Shen, B. H. Li, Z. Z. Zhang, L. Liu, L. G. Zhang, D. Z. Shen, *Appl. Phys. Lett.* 2012, **101**, 011106.
4 (a) K. Y. Cheong, N. Muti, S. R. Ramanan, *Thin Solid Films* 202, **410**, 142; (b) Y. Caglar, S. Ilican, M. Caglar, F. Yakuphanoglu, *J. Sol-Gel Sci. Technol.* 2010, **53**, 372.
5 (a) S. Majumdar, P. Banerji, *Superlatti. Microstruct.* 2009, **45**, 583; (b) M. Wang, E. J. Kim, S. H. Hahn, *J. Lumin.* 2011, **131**, 1428; (c) R. Bhattacharjee, I. -M. Hung, *Mater. Chem. Phys.* 2014, **143**, 693.
6 H. Kanber, R. J. Cipolli, W. B. Henderson, J. M. Whelan, *J. Appl. Phys.* 1985, **57**, 4732.
7 Y. G. Wang, S. P. Lau, X. H. Zhang, H. H. Hng, H. W. Lee, S. F. Yu, B. K. Tay, *J. Cryst. Growth* 2003, **259**, 335.

8 K. Vanheusden, C. H. Seager, W. L. Warren, D. R. Tallant, J. A. Voigt, *Appl. Phys. Lett.* 1996, **68**, 403.

9 (a) D. C. Reynolds, D. C. Look, B. Jogai, C. W. Litton, T. C. Collins, W. Harsch, G. Cantwell, *Phys. Rev. B* 1998, **57**, 12151; (b) G. Xiong, K. B. Ucer, R. T. Williams, J. Lee, D. Bhattacharyya, J. Metson, P. Evans, *J. Appl. Phys.* 2005, **97**, 043528; (c) K. Kitamura, T. Yatsui, M. Ohtsu, G. -C. Yi, *Nanotechnology* 2008, **19**, 175305; (d) D. O. Dumcenco, Y. S. Huang, D. H. Kuo, K. K. Tiong, *J. Lumin.* 2012, **132**, 1890.

10 K. W. Liu, M. Sakurai, M. Aono, *J. Appl. Phys*. 2010, **108**, 043516

11 (a) Y. R. Ryu, T. S. Lee, H. W. White, *Appl. Phys. Lett.* 2003, **83**, 87; (b) D. -K. Hwang, H. -S. Kim, J. -H. Lim, J. -Y. Oh, J. -H. Yang, S. -J. Park, K. -K. Kim, D. C. Look, Y. S. Park, *Appl. Phys. Lett.* 2005, **86**, 151917; (c) F. X. Xiu, Z. Yang, L. J. Mandalapu, D. T. Zhao, J. L. Liu, W. P. Beyermann, *Appl. Phys. Lett.* 2005, **87**, 152101; (d) F. X. Xiu, Z. Yang, L. J. Mandalapu, J. L. Liu, W. P. Beyermann, *Appl. Phys. Lett*. 2006, **88**, 052106; (e) C. X. Shan, Z. Liu, S. K. Hark, *Appl. Phys. Lett.* 2008, **92**, 073103.